https://doi.org/10.3311/PPci.23650

Periodica Polytechnica Civil Engineering, 68(3), pp. 731–741, 2024

Study on Coordinated Deformation Failure Mechanism and Strength Prediction Model of Rock-lining Concrete

Anlong Hu[1], Yalu Sun[1], Yong Wei[1], Zhipeng Shang[1], Xiaoping Wang[2*]

[1] Economic and Technological Research Institute of State Grid Gansu Electric Power Company, Xijin East Road 628., Qilihe District, 730050 Lanzhou, Gansu, China
[2] College of Civil Engineering and Architecture, China Three Gorges University, University Road 8., Xiling District, 443002 Yichang, Hubei, China
[*] Corresponding author, e-mail: 1102544873@qq.com

Received: 16 October 2023, Accepted: 30 January 2024, Published online: 14 March 2024

Abstract

Shotcrete has been widely used in the excavation of caverns and tunnels as a key load-bearing element in the support system. However, the interfacial stresses and bond strengths within the composite structures formed by the interaction of geologic bodies and tectonic formations are not well understood, which can lead to safety accidents and excessive wastage of support materials in engineering. To address this gap, rock-concrete composite specimens were created using six distinct types of surrounding rocks. The strength law of composite specimens was analyzed, and the uniaxial compressive strength prediction model of composite specimens was derived based on Mohr−Coulomb strength yield criterion. The results show that the uniaxial compressive strength of the composite specimen changes with the change of rock type, which is between the strength of rock and concrete. The uniaxial peak strength and elastic modulus of composite specimens are linearly positively correlated with the ratio (*Y*) of concrete-rock elastic modulus, which is easily affected by concrete properties. However, the peak strain is linearly and negatively correlated with *Y*, which is greatly influenced by rock. The rock-concrete interface of the composite specimen plays an important role in the failure of the specimen, which changes the stress transfer state of the composite specimen, produces uncoordinated deformation, and finally causes the failure of the specimen. The theoretical and test value error of the derived composite specimen uniaxial compressive strength prediction model are –1.19%~12.20%, and the theoretical calculation model can be used to predict the uniaxial compressive strength of rock-concrete composite specimens.

Keywords

rock-concrete, composite interface, uniaxial compression, mechanism of destruction, strength prediction

1 Introduction

With the rapid expansion of China's transportation industry, it has emerged as a transportation powerhouse. To accommodate the growing demand for expanded highways, railroads, and municipal engineering lines, tunnels have become integral components. In the process of tunnel construction ground excavation makes the primary rock stress release, stress field redistribution to form a secondary stress field caused by deformation of the tunnel surrounding rock, or even destabilization damage [1]. Thus, concrete lining is usually used as a support structure to control the deformation of the surrounding rock and prevent its destruction [2]. At present, numerous scholars have conducted varying degrees of research on the impact of load [3, 4], structure [5–8], and materials [9–11] on the overall stability of tunnels within the tunnel support system, yielding abundant results. Sun et al. [12] studied the bolt-surrounding rock interaction behavior considering pre-reinforcement. Guan et al. [13] discussed the influence of blasting impact on the stability and interaction of temporary supporting structures such as temporary intermediate walls during tunnel blasting construction. However, in these studies, scholars and designers rarely consider the role of primary lining sprayed concrete in second lining research and design from a safety perspective, resulting in conservative approaches. Primary lining sprayed concrete serves not only to effectively

Cite this article as: Hu, A., Sun, Y., Wei, Y., Shang, Z., Wang, X. "Study on Coordinated Deformation Failure Mechanism and Strength Prediction Model of Rock-lining Concrete", Periodica Polytechnica Civil Engineering, 68(3), pp. 731–741, 2024. https://doi.org/10.3311/PPci.23650

prevent the surrounding rock's exposure to air and water but also rapidly forms on the tunnel's surrounding rock surface, resisting spalling adhesion and providing shear resistance along the contact surface [14]. It can efficiently eliminate the concentration of stress on the excavation surface, forming a supporting counterforce. This leads to the creation of an arch-shaped compressive stress band in the surrounding rock, preventing loosening and inhibiting significant deformation, thus serving a supportive role. The stronger the adhesion bond between the surrounding rock and the sprayed concrete interface, the more pronounced the transfer of compressive stress to the rounding rock through the contact surface. According to the principles of unloading rock mechanics [15–17], this contributes to the stability of the surrounding rock. Zhao et al. [18] believe that the key to study the interaction between surrounding rock and tunnel lining, dam body and dam foundation is the mechanical behavior of the contact surface or contact part of the engineering body and the geological body and the transfer of stress and strain. In order to investigate the interaction between geological bodies and tectonic bodies, a variety of rocks and concrete were used to make two-material models, and a large number of compression and shear tests were carried out [19–22]. Yang et al. [23] developed a three-body model consisting of two geologic bodies and one tectonic body to study how three different materials interact under loads, and thus to explore the response of the ground support system to axial loads in underground space. Zhao et al [24, 25] analyzed the effect of contact surface constraints on the strength and deformation characteristics of composite specimens through triaxial compression tests of sandstone-concrete composite specimens, and the damage mechanism of composite specimens. Selçuk and Aşma [26] carried out uniaxial compression, point load and splitting tests of rock-concrete composite interface at different tilt angles, which showed that the uniaxial compression strength of interface tilted from 0° to 90° varied with the angle of the "U"-shape, and the splitting strength increased with the increase of the angle of the interface. The splitting strength increased with the increase of angle. In addition to laboratory tests, numerical simulation is also of great significance in engineering practice and theoretical research [27]. And scholars have gradually applied numerical simulation methods to the analysis method of lining-surrounding rock interaction. A comprehensive analysis of the aforementioned factors reveals that the properties of the material, contact surface roughness, inclination of the contact position, and mechanical variability of the surrounding rock-primary lining sprayed concrete significantly influence strength and damage mode of the two-medium combination. However, there are insufficient studies on the coordinated deformation mechanism and strength prediction model considering the interaction between shotcrete and surrounding rock. To address this gap, it is imperative to examine the coordinated deformation mechanism among various types of surrounding rock in tunnels and the preliminary lining sprayed concrete. Additionally, it is crucial to summarize the impact of different types of surrounding rock on the stability of tunnel lining, especially considering variations in the stability of the initial lining. Therefore, based on the force mechanism of tunnel surrounding rock and primary lining concrete, generalize the structural form of tunnel vault surrounding rock and primary lining concrete, make a variety of surrounding rock-primary lining concrete composite specimens to carry out uniaxial compression test, to explore the influence of the differences in the mechanical properties of the surrounding rock and concrete materials on the basic mechanical parameters of the two media materials of the combination of the "geologic - engineering body" and combine the composite specimen with the force characteristics and destructive mechanism, and to derive the predictive model of the uniaxial compressive strength, with the aim of providing some useful practical references for the study of the stability of the composite interface of the surrounding rock-primary lining engineering.

2 Experimental overview

2.1 Experimental preparation

Rock specimen production: The rock specimens are made of the widely distributed and representative tunnel surrounding rocks in Chongqing, China. And 6 types of rock blocks, including red sandstone, white sandstone, yellow sandstone, green sandstone, sandy slate, and marble, are selected from different tunnel construction sites. According to *ISRM*, the blocks were drilled, cut, ground and made into standard cylindrical specimens, and in order to minimize the influence of specimen end surface flatness on the test results, the specimen end surface flatness was not more than ±0.03 mm, and the deviation of the two end surfaces from the axis was not more than 0.25°. Rock-concrete composite specimen production: primary lining concrete and surrounding rock contact surface there is resistance to spalling adhesion and along the contact surface of the shear resistance, and in the process of tunnel

excavation with the generation of the critical surface, the maximum principal stress direction of the arch from radial to tangential, increasing the top arch tangential force, and also increasing the risk of tunnelling in the process of the risk of toppling. As we know, the interface between arched tunnel rock and shotcrete is not only subject to the above shear stress, but also to the normal stress of vertical action [28]. Therefore, the generalization of the tunnel vault surrounding rock and the initial lining concrete structure form and force mode, intercept the top arch rock-concrete "key block" as the object of study in Fig. 1, produced a rock – concrete composite specimens. In this paper, only the shear force is considered in the design of the test scheme and the production of rock-concrete composite specimens.

In the preparation of rock-concrete composite specimens. Firstly, six types of surrounding rock complete cylindrical rock specimens (*D* 50 mm × *H* 100 mm) along the diameter direction were cut into semi-cylindrical specimens, and put into the tap water soaking to be completely saturated. Then the rock specimens were put into the diameter of 50 mm, the height of 100 mm cylindrical plastic mold. *P* × *O*42.5 ordinary silicate cement was used as binder material. Natural river sand with maximum particle size not exceeding 2 mm was used as fine aggregate, and granite crushed stone with good grading of 5~10 mm was used as coarse aggregate, and it was formulated into *C*20 concrete. Calculate the required mass of each raw material of concrete according to the ratio, place the weighed raw materials in the mixer and mix them dry, then add water to mix, to be fully mixed, pour the concrete mixture into a plastic mold with a semi-cylindrical rock specimen, placed on the vibration table vibration and compactness, after 24 h of resting, take off the specimen plastic mold and put it into the temperature of 20 ℃ ± 2 ℃, the relative humidity of more than 95% of the standard curing box maintenance for 28 d. The partial process of composite sample processing is shown in Fig. 2 (a). The test

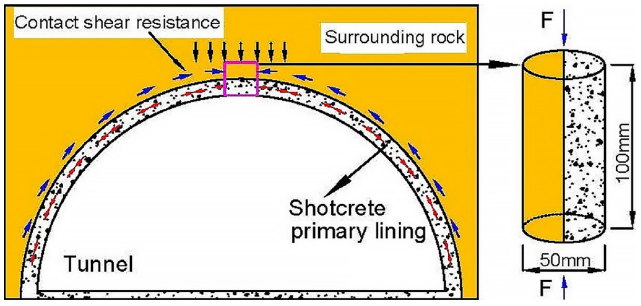

Fig. 1 Cross-sectional resistance of surrounding rock

concrete, rock, rock-concrete composite specimens were produced 1 group, 6 groups, 6 groups, a total of 13 groups, each group of 3 specimens, part of the rock-concrete composite specimens shown in Fig. 2 (b).

2.2 Experimental procedure

For ease of description, the rock specimens were labeled with letters before the start of the test as: red sandstone (*A*), white sandstone (*B*), yellow sandstone (*C*), green sandstone (*D*), slate sandstone (*G*), and marble (*F*). The rock-concrete composite specimens corresponding to the rocks are labeled with a letter and number 1, e.g., red sandstone-concrete (*A1*), and the rest in order: *B1*, *C1*, *D1*, *G1*, *F1*. The strength characteristics and destructive behavior

(a)

(b)

Fig. 2 Process and finished product of rock-concrete composite sample (a) The composite sample processing process (b) Rock-concrete composite specimen

tests of concrete, rock, and rock-concrete composite specimens were completed by using the uniaxial compression function of the *RTR*–1500 rock testing system, which was loaded by a microcomputer-controlled hydraulic servo press, and could be loaded up to a maximum of 1.500 kN. The test loading method was stress-controlled, with a loading rate of 0.05 MPa/s, and axial strain was obtained by a *LVDT* transducer. Fig. 3 shows flow of the experimental process and the organization of the paper framework.

3 Results of the experiment

3.1 Uniaxial compressive stress-strain curve

The succeeding sections of this paper provide a detailed discussion of the experimental results concerning the strength characteristics and damage behavior of concrete, rock, and rock-concrete. In order to quantitatively describe the variability of mechanical properties between the two constituent materials of the rock-concrete composite specimens, the elastic modulus ratio between concrete and rock is introduced to be expressed as *Y*, i.e., $\gamma = E_h/E_r$. The values of uniaxial compressive peak strength, elastic modulus, and peak strain for concrete and six types of rock and composite specimens are shown in Table 1, and the stress-strain curves are shown in Fig. 4.

As can be seen from Table 1, the single specimen strengths in order from low to high are: concrete, yellow sandstone (*C*), white sandstone (*B*), red sandstone (*A*), green sandstone (*D*), slate sandstone (*G*), and marble (*F*). While the composite specimen strengths are overall smaller than the corresponding rock strengths, the strengths of several types of rock composite specimens are in the same order as the corresponding rock specimen strengths, but the composite specimen strengths are all higher than the concrete specimen strengths. The composite specimen (*A*~*F*) decreased by 11.19%, 8.05%, 6.95%, 17.98%, 24.49%, and 21.99%, respectively, compared to the rock strength. While the strength of each composite specimen increased by 30.37%, 22.16%, 11.28%, 39.81%, 56.43%, and 78.23%, respectively, compared to the

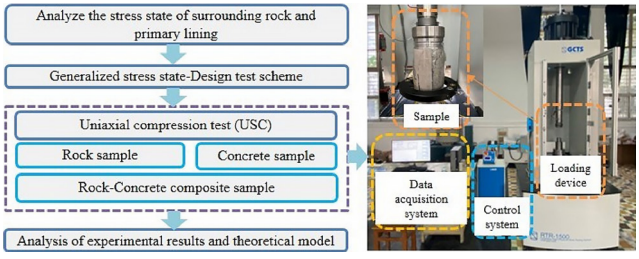

Fig. 3 Test process and organization process

Table 1 The mechanical parameters of specimens

No.	Peak strength σ/ MPa	Elastic modulus *E*/ GPa	Peak strain ε/ %	Ratio of elastic modulus *Y*
H	31.49	9.58	0.44	-
A	46.23	9.08	0.74	-
B	41.84	7.02	0.88	-
C	37.66	6.60	0.93	-
D	53.67	9.86	0.75	-
G	65.23	12.08	0.52	-
F	71.94	16.77	0.44	-
A1	41.05	5.22	0.81	0.95
B1	38.47	4.69	0.92	0.73
C1	35.04	4.02	0.96	0.69
D1	44.02	6.30	0.79	1.03
G1	49.26	8.42	0.62	1.26
F1	56.12	12.30	0.52	1.75

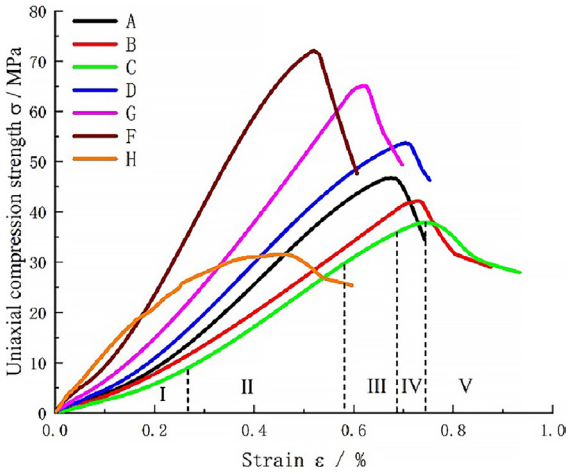

(a)

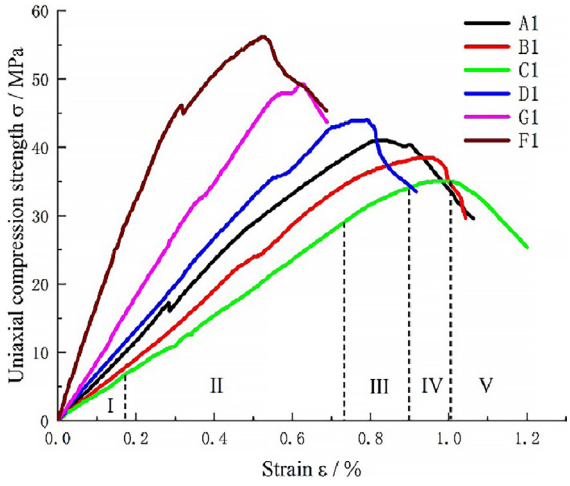

(b)

Fig. 4 Stress-strain curve of uniaxial compression (a) Concrete, rock specimens (b) Concrete-rock composite specimens

concrete specimen strength. It can be seen that the peak strength of rock-concrete composite specimen is between rock strength and concrete strength. The stress-strain curve of the rock specimen, as depicted in Fig. 4, exhibits distinct stages denoted as I to V. Stage I involves fissure compaction, where the original natural pores and fissures of the rock gradually compress. Stage II is characterized by elastic deformation, showcasing linear growth of axial stress and strain.

Stage III marks the onset of stable rupture development, indicating plastic deformation, emergence of micro-ruptures, and an increase in axial strain rate. Stage IV is the unstable rupture stage, signifying the progressive development of rupture. Finally, Stage V represents the destruction stage, depicting rupture surface penetration and strength drop. Composite specimens in the loading process can also be divided into crack compaction, elastic deformation, stable rupture, unstable rupture and destruction of five stages, but in the continuous application of the load process, the curve appeared a "jump", and with the increase of the ratio of the modulus of elasticity of the concrete-rock (Y), the more pronounced the "jump", which indicates that the two materials due to different mechanical properties, resistance to deformation of the ability to differ greatly. Under vertical load, the two materials begin to coordinate deformation to achieve equilibrium. As loading continues, the growing differences in deformation between the two materials result in apparent uncoordinated deformation at the interface, manifesting as misalignment and causing the stress-strain curve to exhibit a distinct "jump."

3.2 Relationship between Ratio of elastic modulus (γ) and mechanical parameters

Fig. 5 shows the elastic modulus ratio of concrete and rock versus peak strength, elastic modulus, and peak strain of composite specimens, respectively. As can be seen in Fig. 5, the peak strength of composite specimens is between rock strength and concrete strength, and closer to concrete strength (weak material); the elastic modulus of composite specimens, except for $G1$ composite specimen, the rest of the composite specimen elastic modulus is less than the concrete elastic modulus, and the peak strain is larger than that of concrete specimen and rock specimen; it shows that the composite specimen's ability to resist deformation is weakened, and deformation is increased. The ratios (γ) of concrete-rock elastic modulus and composite specimen-concrete specimen peak strength, elastic

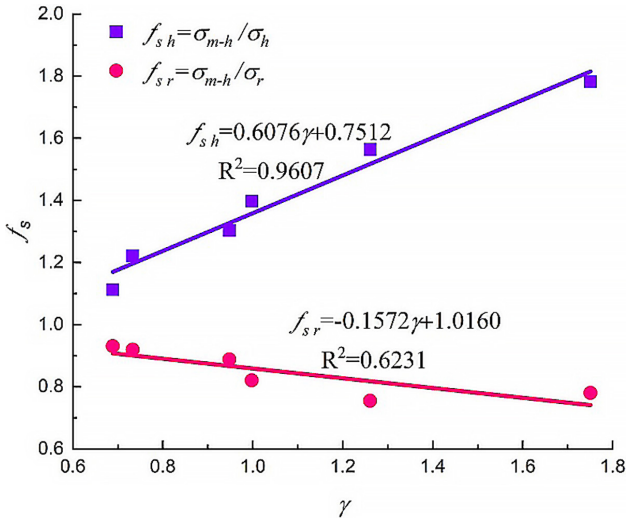

(a)

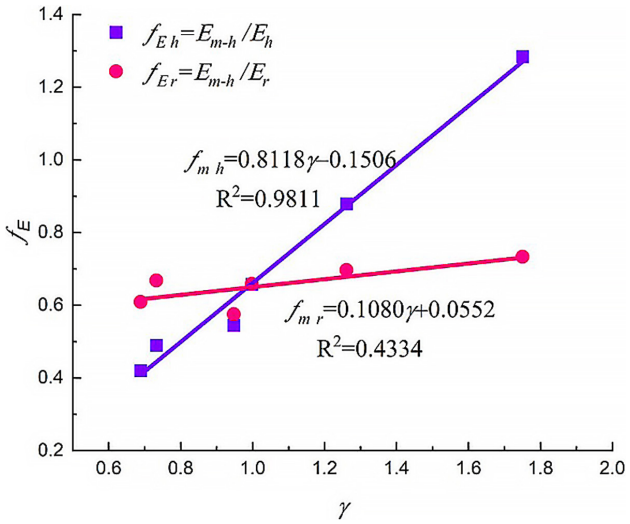

(b)

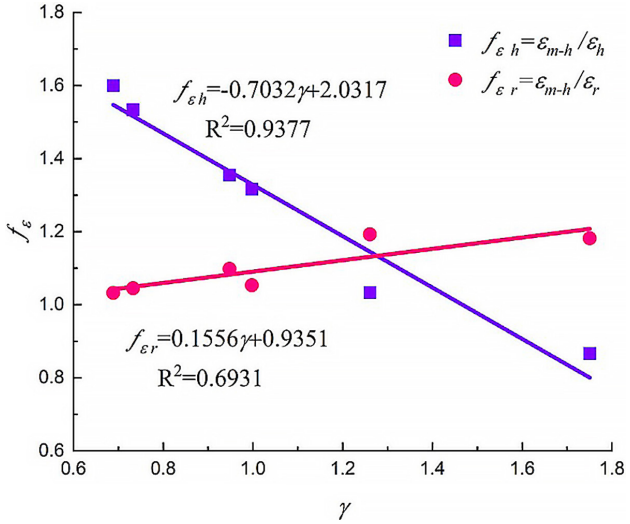

(c)

Fig. 5 Relationship between γ and mechanical properties (a) Uniaxial peak strength (b) Ratio of elastic modulus (c) Peak strain

modulus, peak strain ($f_{sh} = N_{m\text{-}h}/N_{h\text{-}r}$.) show obvious correlation. Among them, the uniaxial peak strength and modulus of elasticity of the composite specimen are linearly positively correlated with the concrete-rock elastic modulus ratio (γ), which increases with the increase of the peak strain decreases with the increase of the peak strain, which is linearly negatively correlated. Therefore, the composite specimen in the loading process, the peak strength, elastic modulus and peak strain are easily affected by the concrete properties, and the elastic modulus is affected by the largest (R^2 = 0.9811), the peak strength of the second (R^2 = 0.9607), the peak strain of the smallest (R^2 = 0.9377).

3.3 Effect of elastic modulus ratio (γ) on damage patterns

Fig. 6 shows the damage morphology of the composite specimen in the uniaxial compressive test. Due to the differences in the mechanical properties of the two materials, different forms of damage occurred, and two main forms of damage occurred.

1. When the modulus of elasticity ratio (γ) between the two materials is less than 1, as observed in specimens *A*1, *B*1, and *C*1, the composite specimen experiences interface cracking. Both materials exhibit a roughly equal number of cracks, with rock damage primarily characterized by shear damage. Vertical cracks appear in the concrete material, accompanied by a small number of tensile cracks.
2. Conversely, when the modulus of elasticity ratio (γ) is greater than or equal to 1, exemplified by specimens *D*1, *G*1, and *F*1, the composite specimen's interface undergoes noticeable damage. Due to substantial lithological differences between the two materials, uncoordinated deformation occurs, and additional friction constraint forces are significant. Consequently, interfacial cracks appear extensively throughout the specimen, eventually leading to interface separation. The number of cracks in concrete exceeds those in rock, with rock predominantly exhibiting splitting cracks and concrete primarily sustaining shear damage.

Under continuous loading, stress concentration occurs at both ends of the composite specimen, and secondary cracks appear at the upper and lower ends of the specimen, or even detachment; while the axial pressure on the center part of the inner ring of the specimen is larger than that of the outer ring. Due to transverse deformation, the specimen experiences tension in both tangential and radial

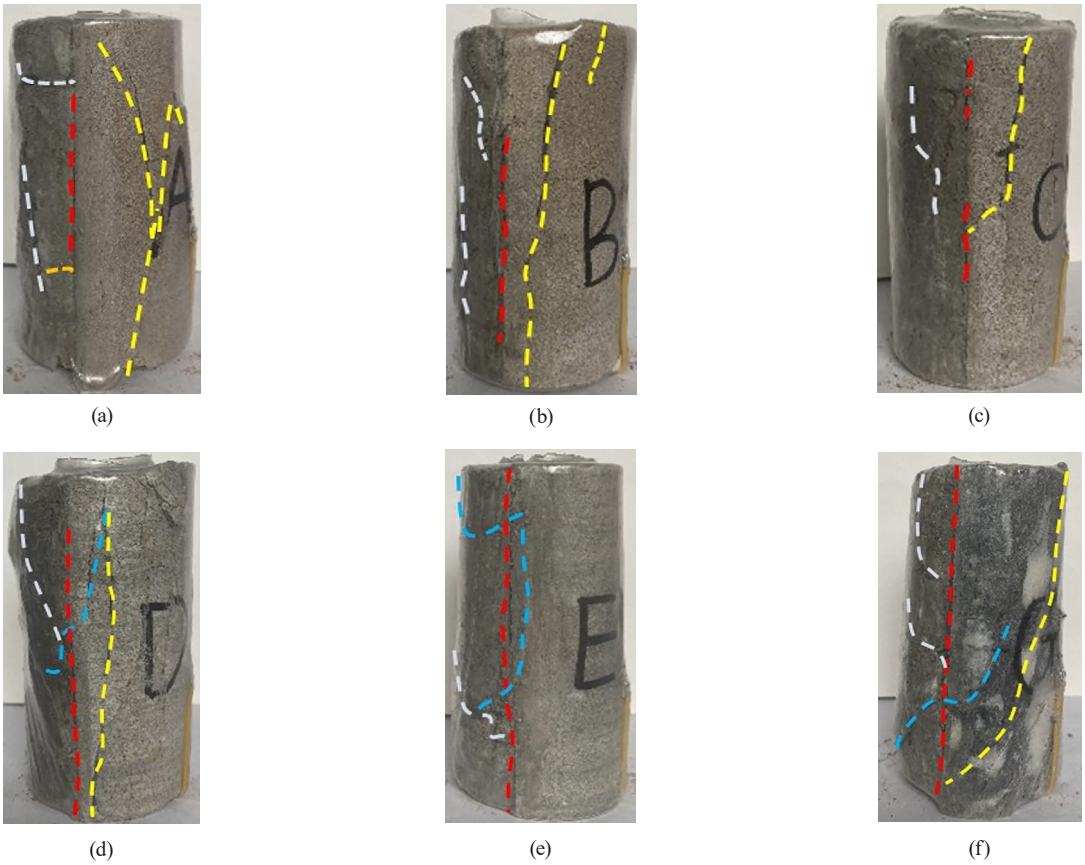

(a) (b) (c)

(d) (e) (f)

Fig. 6 Failure diagram of composite specimen in uniaxial compression test (a) *A*1, (b) *B*1, (c) *C*1, (d) *D*1, (e) *G*1, (f) *F*1

directions, marking the onset of the destructive process. Regardless of whether the modulus of elasticity ratio (γ) is less than or greater than 1, vertical tensile cracks form in the rock-concrete interface, leading to the separation of the two materials.

4 Uniaxial compressive strength prediction model for composite specimens

According to the literature [29] and the above test results as well as the analysis of the damage mechanism of the concrete-rock composite specimen, it can be seen that the composite specimen is subjected to vertical compressive stresses in the vertical direction and lateral tensile stresses in the transverse direction in the case of uniaxial compression, and the force analysis of its unit body is shown in Fig. 7. Assuming that the concrete-rock interface always remains tightly bonded until the composite specimen breaks down, according to the equilibrium condition [30] and generalized Hooke's law, the stress-strain relationship of the unit cell in Fig. 7 can be expressed as Eqs. (1) and (2).

$$\begin{cases} \varepsilon_1 = \varepsilon_{1h} = \varepsilon_{1r} \\ \varepsilon_{2h} = \varepsilon_{2r} = \varepsilon_{3h} = \varepsilon_{3r} \\ \sigma_{2h} = -\sigma_{2r} = \sigma_{3h} = -\sigma_{3r} \end{cases} \tag{1}$$

Where: σ_{1h}, σ_{2h}, σ_{3h}, ε_{1h}, ε_{2h}, ε_{3h} are the stress and strain in the direction of the first, second and third principal stresses of concrete, and σ_{1r}, σ_{2r}, σ_{3r}, ε_{1r}, ε_{2r}, ε_{3r} are the stress and strain in the direction of the first, second and third principal stresses of rock, respectively.

$$\begin{cases} \varepsilon_{1h} = \left[\sigma_{1h} - \mu_h\left(\sigma_{2h} + \sigma_{3h}\right)\right]/E_h \\ \varepsilon_{1r} = \left[\sigma_{1r} - \mu_r\left(\sigma_{2r} + \sigma_{3r}\right)\right]/E_r \\ \varepsilon_{3h} = \left[\sigma_{3h} - \mu_h\left(\sigma_{2h} + \sigma_{1h}\right)\right]/E_h \\ \varepsilon_{3r} = \left[\sigma_{3r} - \mu_r\left(\sigma_{2r} + \sigma_{1r}\right)\right]/E_r \end{cases} \tag{2}$$

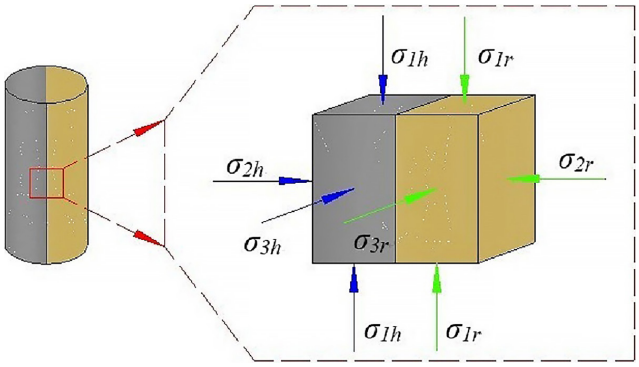

Fig. 7 Force analysis of composite specimen element

Where: μ_h, μ_r is the Poisson's ratio of rock and concrete respectively, E_h, E_r is the elastic modulus of rock and concrete respectively. The association Eqs. (1) and (2) can be obtained, as shown in Eq. (3):

$$\begin{cases} \sigma_{3h} = \dfrac{\left(E_r\ \mu_h - 1/\gamma \times E_h\ \mu_r\right)}{E_r\left(1-\mu_h\right) + E_h\left(1-\mu_r\right)}\sigma_{1h} \\ \sigma_{3r} = \dfrac{\left(\gamma E_r\ \mu_h - 1 - E_h\ \mu_r\right)}{E_r\left(1-\mu_h\right) + E_h\left(1-\mu_r\right)}\sigma_{1r} \end{cases}. \tag{3}$$

From the Mohr-Coulomb yield criterion [31], the shear strength of a material is the sum of the frictional force generated by the rock cohesion c and the normal stress $\sigma_n \times \tan\varphi$ on the shear surface, see Eq. (4):

$$\tau = c + \sigma_n \times \tan\varphi \tag{4}$$

According to the force analysis of the material unit cell in an arbitrary plane, as shown in Fig. 8, it can be deduced that the positive and shear stresses suffered by the unit cell in an arbitrary plane are shown in Eqs. (5) and (6), respectively.

$$\sigma_n = \frac{1}{2}\left(\sigma_1 + \sigma_3\right) + \frac{1}{2}\left(\sigma_1 - \sigma_3\right)\cos 2\beta \tag{5}$$

$$\tau = \frac{1}{2}\left(\sigma_1 - \sigma_3\right)\sin 2\beta \tag{6}$$

This is further shown by the relationship between c and φ shown in Fig. 9 (as shown in Eq. (7)) Moore's Circle and Moore's Circle Envelope:

$$2\beta = 90° + \varphi\ . \tag{7}$$

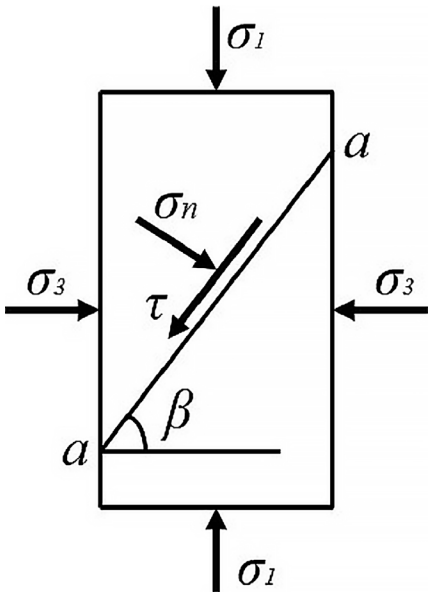

Fig. 8 Force analysis of unit body in any plane

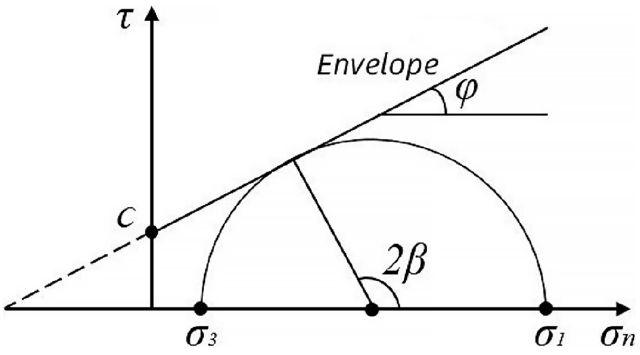

Fig. 9 Mohr circle and Mohr circle envelope

According to Eqs. (4)–(7), the limiting stress equilibrium equations [32, 33] in the two-dimensional state at an arbitrary angle can be obtained as shown in Eq. (8).

$$\sigma_1 = \frac{2c\ \cos\varphi}{1-\sin\varphi} + \frac{1+\sin\varphi}{1-\sin\varphi}\sigma_3 \tag{8}$$

When the material is only subjected to uniaxial compression load $\sigma_3 = 0$, then the uniaxial compression strength of σ_{UCS} the material can be expressed in Eq. (9).

$$\sigma_{UCS} = \frac{2c\cos\varphi}{1-\sin\varphi} \tag{9}$$

Rock-concrete composite specimen due to the differences in the mechanical properties of the two materials, there is the emergence of unbalanced forces, so there is a mutual constraint effect between the interfaces. So the concrete-rock interface can be regarded as a three-way state of force, and then the joint Eqs. (3) and (9) to obtain the compressive strength of the rock and concrete in the composite specimen, that is shown in Eq. (10).

$$\begin{cases} \sigma_{1h} = \sigma_{USC-h} + \dfrac{1+\sin\varphi_h}{1-\sin\varphi_h} \times \dfrac{\left(E_r\mu_h - 1/\gamma \times E_h\mu_r\right)}{E_r\left(1-\mu_h\right) + E_h\left(1-\mu_r\right)}\sigma_{1h} \\ \sigma_{1r} = \sigma_{USC-r} + \dfrac{1+\sin\varphi_r}{1-\sin\varphi_r} \times \dfrac{\left(\gamma E_r\mu_h - E_h\mu_r\right)}{E_r\left(1-\mu_h\right) + E_h\left(1-\mu_r\right)}\sigma_{1r} \end{cases} \tag{10}$$

Let $a_h = \dfrac{1+\sin\varphi_h}{1-\sin\varphi_h}$, $b_h = \dfrac{\left(E_r\mu_h - 1/\gamma \times E_h\mu_r\right)}{E_r\left(1-\mu_h\right) + E_h\left(1-\mu_r\right)}$,

$a_r = \dfrac{1+\sin\varphi_r}{1-\sin\varphi_r}$, $b_r = \dfrac{\left(\gamma E_r\mu_h - E_h\mu_r\right)}{E_r\left(1-\mu_h\right) + E_h\left(1-\mu_r\right)}$. Where φ_h, φ_r are the angle of internal friction between concrete and rock, respectively, the uniaxial compressive strength of the composite specimen can be obtained by simplifying Eq. (11).

$$\sigma_1 = \frac{1}{2} \times \left(\frac{\sigma_{UCS-h}}{1-a_h b_h} + \frac{\sigma_{UCS-r}}{1-a_r b_r} \right) \tag{11}$$

Where $\sigma_{UCS\text{-}h}$, $\sigma_{UCS\text{-}r}$ are the uniaxial compressive strengths of concrete and rock, respectively.

5 Discussions

The rock-concrete interface assumes a pivotal role in specimen damage, and the force analysis and damage mechanism at the composite layer cementation are intricate, often dictated by differences in the mechanical properties of the two materials. During compression, the material with a higher modulus of elasticity generates a greater radial compressive stress, whereas the material with a smaller modulus of elasticity experiences a reduced radial compressive stress. This creates an unbalanced force between the materials, causing the material with a higher modulus to exert an extrusion effect on the material with a lower modulus. Consequently, there is a decrease in the lateral strain of the material with a smaller modulus near the contact interface and an increase in the lateral strain of the material with a higher modulus. According to Hooke's law, with the same axial strain, the change in lateral strain amplifies the lateral stress of the material with a smaller elastic modulus and diminishes the lateral stress of the material with a larger elastic modulus.

In the compression process of composite specimens, there is a transfer of strain and stress between the two materials. This transfer coordinates the unbalanced force and deformation generated by the material with a strong elastic modulus and the weak material. Despite the reduction in unbalanced force through the transfer of stress and strain, the material with a higher modulus of elasticity continues to bear the main load during the loading process, producing a substantial radial stress and resulting in the persistence of unbalanced force. This ultimately leads to significant uncoordinated deformation and specimen damage. Hence, the radial stress of materials with a higher modulus of elasticity significantly influences the reduction in the strength of composite specimens.

In this paper, the test result value of literature [33] and the calculated value of the strength prediction model of the concrete-surrounding rock composite specimen proposed were selected for verification and analysis, and the result values of the two were compared as shown in Fig. 10. From Fig. 10, it can be concluded that the uniaxial compressive strength calculated by the composite

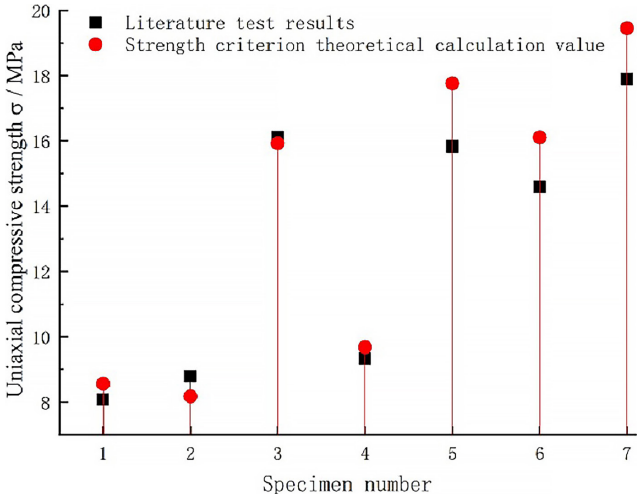

Fig. 10 Comparison of uniaxial compressive strength test values and theoretical calculated values

specimen strength prediction model is relatively close to the experimental compressive strength value measured directly, with an error value of –1.19% to 12.20%, which is basically in line with the two, indicating that the applicability of the uniaxial compressive strength prediction model of the composite concrete-enclosed rock specimen proposed in this paper is strong. In summary, the research results of this paper, on the one hand, for the different geological formations of the surrounding rock and concrete initial support of the interaction mechanism and damage mechanism for a detailed analysis; on the other hand, the composite specimen uniaxial compressive strength prediction model can be derived to calculate the uniaxial compressive strength of one of the two media materials, for the design of the initial support of the sprayed concrete ratio and the design of the weak location of the crushed surrounding rock to provide theoretical support. Theoretical support. Although the uniaxial compressive strength of the composite specimen can be obtained according to some basic mechanical parameters, it is not universally applicable, and it is necessary to carry out the uniaxial and triaxial compression tests of concrete specimens of various lithologies and different strength grades to obtain the complete mechanical parameters in the subsequent research work, so as to improve the relevant theories and enhance the accuracy of the model.

6 Conclusions

This study investigates the uncoordinated deformation and damage mechanism of the composite interface in the "geological body-engineering body" lining structure during tunneling construction through the uniaxial compression of rock-concrete composite specimens. Utilizing the generalized Hooke's law, a strength prediction model for rock-concrete composite specimens under uniaxial compression is proposed. This model unveils the force and deformation characteristics of the "geological body-engineering body" lining structure in tunneling construction, yielding the following key conclusions:

1. The uniaxial compressive strengths of different perimeter rock-concrete composite specimens are intermediate between the rock and concrete strengths, increasing with increasing rock strength but closer to the concrete (weak material) strength.
2. The ratio of rock-concrete elastic modulus (γ) is linearly and positively correlated with the ratio of composite specimen-concrete specimen peak strength and elastic modulus ($f_{sh} = N_{m\text{-}h}/N_{h\text{-}r}$), while it is obviously linearly and negatively correlated with peak strain. The uniaxial compressive strength, modulus of elasticity and peak strain of the composite specimen are strongly influenced by the concrete properties.
3. The mechanical property disparity between the two materials affects the composite specimen, with the transfer of strain and stress coordinating the unbalanced force generated during compression between the strong and weak materials. Despite increasing unbalanced force under continuous loading, the coordination ability is limited. Consequently, the composite specimen experiences uncoordinated deformation damage along the bond interface. Hence, the bond strength of the composite interface plays a crucial role in specimen destruction.
4. The compressive strength expression of the rock-concrete composite specimen was established, which quantitatively expressed the stress of each material of the composite specimen. The theoretical calculated values of the uniaxial compressive strength prediction model of the composite specimen are in good agreement with the experimental values, with the errors ranging from –1.19% to 12.20%. The expression can be used to calculate the compressive strength of rock-concrete composite specimens.

Acknowledgement

The authors would like to thank the Key Laboratory of Geological Hazards on Three Gorges Reservoir Area, Ministry of Education for providing all the facilities.

References

[1] Wang, J. F., Huang, H. W., Xie, X. Y., Bobet, A. "Void-induced liner deformation and stress redistribution", Tunnel and Underground Space Technology, 40, pp. 263–276, 2014. https://doi.org/10.1016/j.tust.2013.10.008

[2] Li, C. C. "Principles and methods of rock support for rockburst control", Journal of Rock Mechanics and Geotechnical Engineering, 13(1), pp. 46–59, 2021. https://doi.org/10.1016/j.jrmge.2020.11.001

[3] Taghizadeh, H., Zare, S., Mazraehli, M. "Analysis of rock load for tunnel lining design", Geotechnical and Geological Engineering, 38(3), pp. 2989–3005, 2020. https://doi.org/10.1007/s10706-020-01202-y

[4] Cheng, R. S., Chen, W. S., Hao, H., Li, J. D. "A state-of-the-art review of road tunnel subjected to blast loads", Tunnel and Underground Space Technology, 112, 103911, 2021. https://doi.org/10.1016/j.tust.2021.103911

[5] Song, K. I., Cho, G. C., Chang, S. B., Lee, I. M. "Beam–spring structural analysis for the design of a tunnel pre-reinforcement support system", International Journal of Rock Mechanics and Mining Sciences, 59, pp. 139–150, 2013. https://doi.org/10.1016/j.ijrmms.2012.12.017

[6] Liu, H. Y., Small, J. C., Carter, J. P., Williams, D. J. "Effects of tunnelling on existing support systems of perpendicularly crossing tunnels", Computers and Geotechnics, 36(5), pp. 880–894, 2009. https://doi.org/10.1016/j.compgeo.2009.01.013

[7] Wang, X. L., Lai, J. X., Garnes, R. S., Luo, Y. B. "Support system for tunnelling in squeezing ground of qingling-daba mountainous area: A case study from soft rock tunnels", Advances in Civil Engineering, 2019, Article ID 8682535, 2019. https://doi.org/10.1155/2019/8682535

[8] Sun, Z. Z., Zhang, Y. M., Yuan, Y., Mang, H. A. "Stability analysis of a fire-loaded shallow tunnel by means of a thermo-hydro-chemo-mechanical model and discontinuity layout optimization", International Journal for Numerical and Analytical Methods in Geomechanics, 43(5), pp. 2551–2564, 2019. https://doi.org/10.1002/nag.2991

[9] Sui, Q. R., He, M. C., Shi, T. T., Pang, S. H., Xiang, J. Y., Tao, Z. G., Qu, D. J. "Lateral damage mechanism of the double-track tunnel in the mountainous layered soft rock and NPR anchor cable control", Underground Space, 12, pp. 31–43, 2023. https://doi.org/10.1016/j.undsp.2022.10.011

[10] Wang, X. L., Fan, F. F., Lai, J. X., Xie, Y. L. "Steel fiber reinforced concrete: A review of its material properties and usage in tunnel lining", In Structures. 34, pp. 1080–1098, 2021. https://doi.org/10.1016/j.istruc.2021.07.086

[11] Voit, K., Zimmermann, T. "Characteristics of selected concrete with tunnel excavation material", Construction and Building Materials, 101, pp. 217–226, 2015. https://doi.org/10.1016/j.conbuildmat.2015.10.016

[12] Sun, Z. Y., Zhang, D. L., Fang, Q., Dui, G. S., Tai, Q. M., Sun, F. W. "Analysis of the interaction between tunnel support and surrounding rock considering pre-reinforcement", Tunnel and Underground Space Technology, 115, 104074, 2021. https://doi.org/10.1016/j.tust.2021.104074

[13] Guan, X. M., Yang, N., Zhang, W. J., Li, M. G., Liu, Z. L., Wang, X. H., Zhang, S. L. "Vibration response and failure modes analysis of the temporary support structure under blasting excavation of tunnels", Engineering Failure Analysis, 136(15), 106188, 2022. https://doi.org/10.1016/j.engfailanal.2022.106188

[14] Wen, J. Z., Zhang, Y. X., Wang, C. "Analysis on interfacial stress between surrounding rock and shotcrete lining", Journal of Civil, Architectural & Environmental Engineering, 34(6), pp. 67–74, 2012. (in Chinese) https://doi.org/10.3969/j.issn.1674-4764.2012.06.012

[15] Li, J. L. "Unloading rock mechanics", China Water Resources and Electric Power Press, 2013. ISBN 978-7-5084-1621-2 (in Chinese)

[16] Li, J. L., Huang, T. Z., Zhang, H. B., Deng, H. F. "Reserch review and prospect in experimental studies for unloading rock mass mechanics", Journal of China Three Gorges University (Natural Sciences), 1, pp. 1–13, 2022. (in Chinese) https://doi.org/10.13393/j.cnki.issn.1672-948x.2022.01.001

[17] Wang, L. H., Huang, T. Z., Li, J. L., Zhou, X., Xu, X. L. "Model test research on stress response of high and steep slopes with structural planes during excavation unloading", Chinese Journal of Rock Mechanics and Engineering, 42(08), pp. 1866–1877, 2023. (in Chinese)

[18] Zhao, Z. H., Wang, W. M., Dai, C. Q., Yan, J. X. "Failure characteristics of three-body model composed of rock and coal with different strength and stiffness", Transactions of Nonferrous Metals Society of China, 24(5), pp. 1538–1546, 2014. https://doi.org/10.1016/S1003-6326(14)63223-4

[19] Tian, H. M., Chen, W. Z., Yang, D. S., Yang, J. P. "Experimental and numerical analysis of the shear behaviour of cemented concrete–rock joints", Rock Mechanics and Rock Engineering, 48, pp. 213–222, 2015. https://doi.org/10.1007/s00603-014-0560-6

[20] Yi, C., Zhu, H. G., Wang, H. T., Liu, Z., Pan, H. "Analysis of transformation conditions and influence factors of uni-body and bi-body models under axial compression", Rock and Soil Mechanics, 32(5), pp. 1297–1376, 2011. (in Chinese) https://doi.org/10.16285/j.rsm.2011.05.004

[21] Badika, M., Merabi, B., Capdevielle, S., Dufour, F., Saletti, D. Briffaut, M. "Influence of concrete-rock bonds and roughness on the shear behavior of concrete-rock interfaces under low normal loading, experimental and numerical analysis", Applied Science, 12(11), 5643, 2022. https://doi.org/10.3390/app12115643

[22] Shen, Y. J., Wang, Y. Z., Yang, Y., Sun, Q., Luo, T., Zhang, H. "Influence of surface roughness and hydrophilicity on bonding strength of concrete-rock interface", Construction and Building Materials, 213, pp. 156–166, 209. https://doi.org/10.1016/j.conbuildmat.2019.04.078

[23] Yang, S., Zhang, N., Kan, J. G., Feng, X. W., Pan, D. J., Zhao, Q. F. "Interaction between geological body and structural body in a three-body model", Journal of Central South University, 24(12), pp. 2877–2893, 2017. https://doi.org/10.1007/s11771-017-3702-7

[24] Zhao, B. Y., Liu, Y., Huang, T. Z., Wang, X. P. "Experimental study on strength and deformation characteristics of rock–concrete composite specimens under compressive condition", Geotechnical and Geological Engineering, 37, pp. 2693–2706, 2019.
https://doi.org/10.1007/s10706-018-00787-9

[25] Zhao, B. Y., Liu, Y., Liu, D. Y., Huang, W., Wang, X. P., Yu, G. B., Liu, S. "Research on the influence of contact surface constraint on mechanical properties of rock-concrete composite specimens under compressive loads", Frontiers of Structural and Civil Engineering, 14, pp. 322–330, 2020.
https://doi.org/10.1007/s11709-019-0594-7

[26] Selçuk, L., Aşma, D. "Experimental investigation of the rock–concrete bi materials influence of inclined interface on strength and failure behavior", International Journal of Rock Mechanics and Mining Sciences, 123, 104119, 2019.
https://doi.org/10.1016/j.ijrmms.2019.104119

[27] Zhang, Y. M., Zhuang, X. Y. "Cracking elements method for dynamic brittle fracture", Theoretical and Applied Fracture Mechanics, 102, pp. 1–9, 2019.
https://doi.org/10.1016/j.tafmec.2018.09.015

[28] Zhang, J. L., Liu, X., Ren, T. Y., Yuan, Y., Mang, H. A. "Structural behavior of reinforced concrete segments of tunnel linings strengthened by a steel-concrete composite", Composites Part B: Engineering, 178, 107444, 2019.
https://doi.org/10.1016/j.compositesb.2019.107444

[29] Xian, X. F., Tan, X. S. "Failure mechanism of stratified rock mass", Chongqing University Press, 1989. ISBN 7-5624-0205-1 (in Chinese)

[30] Zhao, J. "Applicability of Mohr–Coulomb and Hoek–Brown strength criteria to the dynamic strength of brittle rock", International Journal of Rock Mechanics and Mining Sciences, 37(7), pp. 1115–1121, 2000.
https://doi.org/10.1016/S1365-1609(00)00049-6

[31] Si, X. F., Gong, F. Q., Li, X. B., Wang, S. Y., Luo, S. "Dynamic Mohr–Coulomb and Hoek–Brown strength criteria of sandstone at high strain rates", International Journal of Rock Mechanics and Mining Sciences, 115, pp. 48–59, 2019.
https://doi.org/10.1016/j.ijrmms.2018.12.013

[32] Chen, M., Cui, X. W., Yan, X., Wang, H., Wang, E. L. "Prediction model for compressive strength of rock-steel fiber reinforced concrete composite layer", Rock and Soil Mechanics, 42(3), pp. 638–646, 2021.
https://doi:10.16285/j.rsm.2020.5571

[33] Wang, W. Q., Ye, Y., Wang, Q. H., Luo, B. Y., Wang, J., Liu, Y. "Interaction and mechanical effect of materials interface of contact zone composite samples: Uniaxial compression experimental and numerical studies", Geomechanics and Engineering, 21(6), pp. 571–582, 2020.
https://doi.org/10.12989/gae.2020.21.6.571